THE JOURNAL OF PHYSICAL CHEMISTRY C

Article

Cite This: J. Phys. Chem. C 2018, 122, 6947−6954

pubs.acs.org/JPCC

Structural Evolution of Gold-Doped Bismuth Clusters $AuBi_n^-$ (n = 4−8)

Seema Pande,[†,∥] Tian Jian,[‡,∥] Navneet Singh Khetrapal,[†] Lai-Sheng Wang,[‡,*] and Xiao Cheng Zeng[†,§,*]

[†]Department of Chemistry, University of Nebraska-Lincoln, Lincoln, Nebraska 68588, United States

[‡]Department of Chemistry, Brown University, Providence, Rhode Island 02912, United States

[§]Department of Chemical & Biomolecular Engineering & Department of Mechanical & Materials Engineering, University of Nebraska-Lincoln, Lincoln, Nebraska 68588, United States

Supporting Information

ABSTRACT: The structures of gold-doped bismuth clusters, $AuBi_n^-$ (n = 4−8), are investigated through a joint photoelectron spectroscopy and density functional theory (DFT) study. Well-resolved photoelectron spectra are obtained at several photon energies. Global minimum searches coupled with DFT calculations yield low-lying structures, whose relative energies are further evaluated by single-point energy calculations at the CCSD(T) level of theory. Vertical detachment energies are calculated with the inclusion of spin−orbit effects to compare with the experimental data. Three-dimensional structures are found to be dominant in this size range, while a planar low-lying isomer is observed only for $AuBi_4^-$. The $AuBi_6^-$ cluster possesses a "bow-tie-like" global minimum structure. Major isomers of the other clusters studied here can all be viewed to possess this structural motif. The gold dopant favors increasingly higher coordination with bismuth in $AuBi_n^-$ (n = 4−8). Chemical bonding analyses are performed to understand the geometric and electronic structure evolution of these bimetallic clusters. The gold atom interacts with neighboring bismuth atoms via localized σ bonds at low-coordination sites but via delocalized σ bonds at high-coordination sites. Greater charge transfer from Bi to Au is found for higher-coordinated Au. Molecular dynamics simulations indicate that the assigned global minimum of $AuBi_7^-$ is a highly stable structure, whereas the minor isomer of $AuBi_7^-$ displays a fluxional behavior.

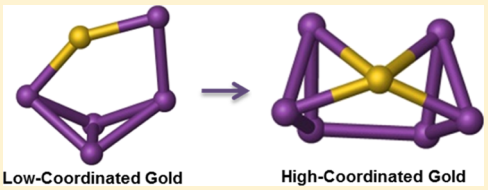

INTRODUCTION

Clusters exhibit unique size-dependent physical and chemical properties that differ from their bulk counterparts. These size-dependent properties in bimetallic clusters depend on various factors such as additional degrees of freedom and composition, chemical interactions among different elemental atoms, or other alloying effects, which may result in increased stability or improved catalytic activity.[1−5] Hence, bimetallic clusters have attracted increasing attention because of their higher flexibility in attaining tunable properties. In this article, we present a joint experimental and theoretical study of bismuth anions doped with single gold atom, $AuBi_n^-$ (n = 4−8).

Bismuth nanoparticles have been shown to exhibit size-dependent superconductivity.[6] The electronic structures and bonding characters of Bi clusters (neutral, anionic, and cationic) have been investigated by photoelectron spectroscopy (PES)[7−14] and theoretical calculations.[15−20] There have been few combined experimental and theoretical studies on bismuth clusters. Gausa et al. performed both PES measurement and theoretical calculations for anionic bismuth clusters and reported a rooflike and a planar ring structure for bismuth tetramer and pentamer, respectively.[21] Kelting et al. used both gas-phase ion mobility spectrometry and trapped-ion diffraction measurements along with density functional theory (DFT) calculations to probe the structures of small-sized bismuth cluster cations.[22] Overall, small bismuth clusters are shown to exhibit more compact structures, whereas the larger clusters are more open and they are formed by the combination of four-, six-, or eight-atom clusters.

There have been numerous investigations on bismuth clusters doped with main group elements,[5,23−32] and a few theoretical studies of bimetallic clusters of bismuth with transition metals have been reported.[33−36] Specifically, recent articles of copper−bismuth binary systems provide an insight into the intermetallic dynamics.[37,38] Also, the combined experimental and theoretical study for tin−bismuth clusters was reported by Heiles et al.[39,40] Bimetallic cluster with gold[41−45] has attracted more attention as small gold clusters are known to possess unique catalytic properties.[46] We are aware of only two theoretical studies on neutral gold−bismuth clusters.[35,36] Our previous PES study of $AuBi^-$ and $BiBO^-$ revealed similarity in the electronic structure and bonding of gold and boronyl to bismuth.[31]

Here, we report the first combined PES and theoretical investigation of gold-doped bismuth anion clusters $AuBi_n^-$ (n = 4−8). The structure evolution in these small bimetallic clusters

Received: January 5, 2018
Revised: February 25, 2018
Published: March 1, 2018

DOI: 10.1021/acs.jpcc.8b00166
J. Phys. Chem. C 2018, 122, 6947−6954

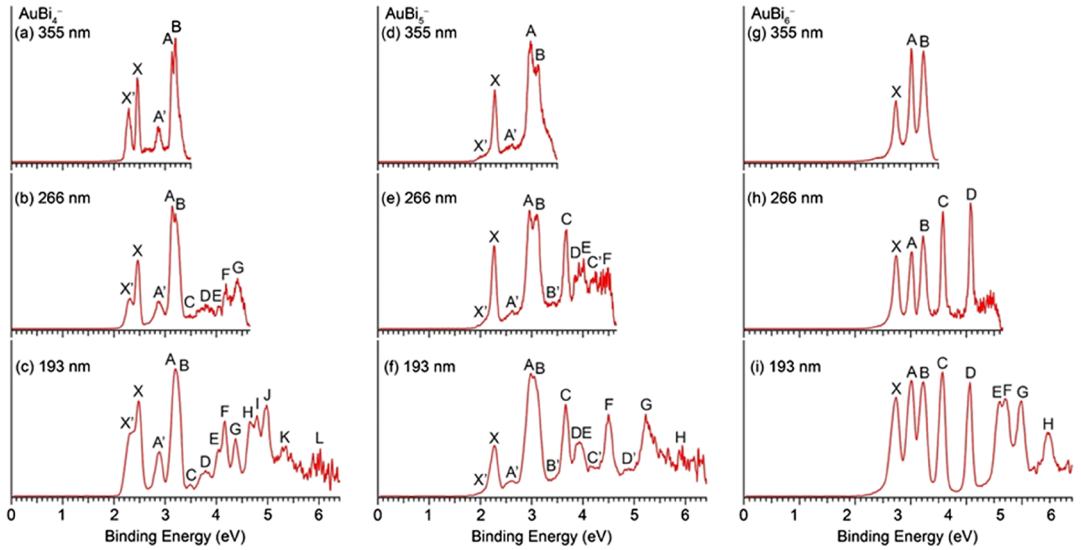

Figure 1. Photoelectron spectra of $AuBi_4^-$ at (a) 355 nm, (b) 266 nm, and (c) 193 nm; $AuBi_5^-$ at (d) 355 nm, (e) 266 nm, and (f) 193 nm; and $AuBi_6^-$ at (g) 355 nm, (h) 266 nm, and (i) 193 nm detachment photon energies.

has been elucidated. Knowledge obtained from this study will pave the way for future studies of larger and more complex bimetallic Au−Bi clusters, which may exhibit novel chemical and physical properties.

METHODS

Experimental Method. The experiments were performed using a magnetic-bottle PES apparatus equipped with a laser vaporization supersonic cluster source, details of which have been published elsewhere.[47,48] Briefly, bimetallic gold−bismuth cluster anions were produced by laser vaporization of an Au/Bi mixed target. A high-pressure helium carrier gas seeded with 5% argon was used to quench the plasma, initiate nucleation, and cool the clusters via supersonic expansion. The gold−bismuth cluster anions were extracted perpendicularly from the cluster beam and analyzed by a time-of-flight mass spectrometer. Clusters of interest were mass-selected, decelerated, and photodetached by the 193 nm (6.424 eV) radiation from an ArF excimer laser and the fourth harmonic (266 nm, 4.661 eV) and third harmonic (355 nm, 3.496 eV) from a Nd:YAG laser. Photoelectrons were collected at nearly 100% efficiency by a magnetic bottle and analyzed in a 3.5 m long electron flight tube. Photoelectron spectra were calibrated using the known spectra of Au^- and Bi^-. The energy resolution of the apparatus was $\Delta E_k/E_k \approx 2.5\%$, that is, approximately 25 meV for 1 eV electrons, where E_k is the kinetic energy and ΔE_k is the change in kinetic energy of the electron.

Theoretical Methods. Global optimization with the basin-hopping (BH) method[49,50] combined with DFT is used to search the low-lying and global minimum structures of each cluster. For the BH-DFT search, we used generalized gradient approximation (GGA) with the Perdew−Burke−Ernzerhof (PBE)[51] exchange correlation functional and double numerical polarized basis set as implemented in DMOL 4.0 program.[52] We used several initial geometries and employed 1.0×10^{-6} Hartree energy convergence, 2×10^{-3} Å gradient convergence, and 5.0×10^{-3} Å displacement convergence for geometry optimization.

Top 10−15 low-lying isomers obtained from the BH search were considered as the candidates for the global minimum. These candidates were reoptimized using meta-GGA M06 functional[53] and the aug-cc-pVTZ (effective core potential, ECP)[54−56] basis set, as implemented in Gaussian 09 package.[57] We optimized these isomers at the lowest spin multiplicity as well as two higher multiplicities. Frequency calculations were done to verify that the isomers were true minima on the potential energy surface. The inclusion of spin−orbit (SO) effects is essential for both gold and bismuth,[30,58] and previous studies on gold or gold-doped clusters have shown that inclusion of SO effects provided quantitatively better theoretical data for comparison with experimental PES spectra.[59−61] Next, single-point energies of these candidate isomers were calculated at the SODFT level using the PBE0 functional[62] and the CRENBL (ECP)[63] basis set, as implemented in the NWCHEM 6.3 package.[64] The SO effects were included for both gold and bismuth in these calculations.[63]

The first vertical detachment energy (VDE) of a cluster was calculated as the energy difference between the neutral and anionic clusters at the optimized structure of the anion. The higher VDEs were calculated by adding vertical excitation energies to the first VDE. Each VDE was then fitted with a unit-area Gaussian of 0.05 eV width to yield the simulated PES spectrum. The global minimum structure was identified by comparing the experimental PES spectrum with the simulated spectra of the low-lying isomers. We also performed coupled-cluster calculations [CCSD(T)] with the aug-cc-pVDZ (ECP) basis set to support the credibility of the assigned isomers. Further, for a quantitative support, we calculated the root-mean-square deviation (rmsd) for the assigned major isomers. We aligned the first peak of the simulated spectra with experimental first VDE and calculated the rmsd of next three peaks of the simulated spectra with respect to the corresponding experimental peaks. The overall theoretical approaches appear to be quite reliable in identifying the global minimum clusters even in the cases where the simulated spectra of more than one candidate isomer exhibit resemblance to the experimental spectrum, as also shown previously.[59−61] Additionally, for two $AuBi_7^-$ isomers, we performed Born−Oppenheimer molecular dynamic (BOMD) simulations at 300 and 260 K for 5 ps with a time step of 1 fs, using the CP2K software.[65] We also performed chemical bonding analyses using

DOI: 10.1021/acs.jpcc.8b00166
J. Phys. Chem. C 2018, 122, 6947−6954

the AdNDP[69] method at the PBE0/Def2-TZVP (ECP) level of theory.

RESULTS AND DISCUSSION

The experimental photoelectron spectra of $AuBi_n^-$ (n = 4−8) are shown in Figures 1 and 2 at three detachment photon

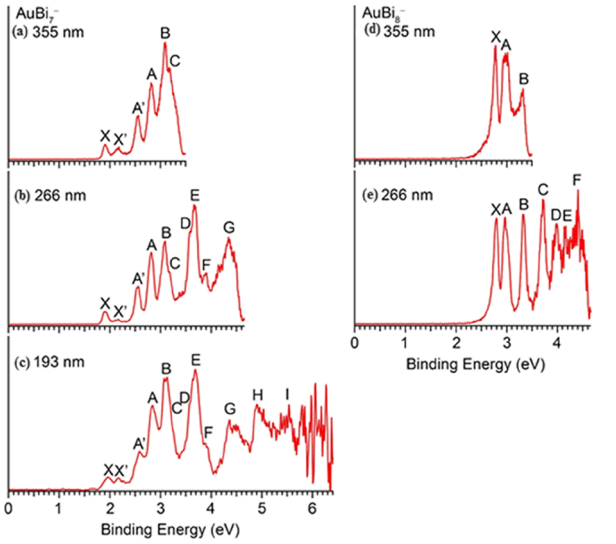

Figure 2. Photoelectron spectra of $AuBi_7^-$ at (a) 355 nm, (b) 266 nm, and (c) 193 nm and $AuBi_8^-$ at (d) 355 nm and (e) 266 nm detachment photon energies.

energies: 355 nm (3.496 eV), 266 nm (4.661 eV), and 193 nm (6.424 eV). Many detachment transitions were observed for each cluster and were labeled by letters.

The X band in each spectrum represents the transition from the ground state of the anion to that of the neutral, whereas bands A, B, ... stand for the transitions to the excited states of the neutral species. Weaker features labeled with X′, A′, B′, ... indicate they are from minor isomers. The experimental first VDEs and the energy gap (energy difference between X and A peaks) are given in Table 1, along with the theoretical first VDEs and relative energies calculated at the CCSD(T) level of theory for the top candidates. The considerable shift to the lower binding energy side is normally observed in the theoretical VDEs with respect to the experiment and is attributed to the SO coupling used for the theoretical calculations.

Table 1. Experimental First VDE (eV) labeled X and X′ in Figure 1 and 2, the Energy Gap (eV) between Bands Labeled X and A or Bands Labeled X′ and A′ in Figure 1 and 2 for $AuBi_n^-$ (n = 4−8), Theoretical First VDE, Point Group, and Relative Energies eV at CCSD(T)/aug-cc-pVDZ (ECP) Level for Top Isomers of $AuBi_n^-$ (n = 4−8)

	experimental		theoretical			
	VDE	gap	isomer	VDE	point group	ΔE
$AuBi_4^-$	2.29 (X′)	0.56	I	1.83	C_{2v}	0.00
	2.45 (X)	0.68	II	1.98	D_{2h}	0.16
			III	2.35	C_s	0.17
$AuBi_5^-$	2.28 (X)	0.70	I	1.96	C_s	0.00
	∼2.0 (X′)	∼0.6	II	1.93	C_s	0.11
$AuBi_6^-$	2.73 (X)	0.28	I	2.26	C_s	0.00
			II	2.47	C_{2v}	0.30
$AuBi_7^-$	1.91 (X)	0.90	I	1.54	C_1	0.00
	2.16 (X′)	0.39	II	1.74	C_s	0.08
$AuBi_8^-$	2.78 (X)	0.19	I	2.36	C_s	0.00
			II	2.19	C_1	0.18
			III	1.98	C_1	0.20

In Figures 3 and 4, the simulated spectra of the top two or three lowest-lying isomers are compared with the experimental spectrum of each anionic cluster. The structures and simulated spectra of other low-lying isomers are presented in the Supporting Information.

$AuBi_4^-$. The 355 nm spectrum of $AuBi_4^-$ (Figure 1a) displays two relatively weak bands (X′ and A′) and three intense bands (X, A, and B). The 266 nm spectrum (Figure 1b) is quite congested at the higher binding energy side. The 193 nm spectrum (Figure 1c) reveals three prominent bands (H−J) and two weak bands (K and L). The spectra of $AuBi_4^-$ indicate that they are from two potential isomers populated in the cluster beam.

Figure 3a presents the theoretical spectra of the three lowest-lying isomers I, II, and III (energy ranking is based on the CCSD(T)/aug-cc-pVDZ (ECP) level of theory). Isomer I is the lowest-energy isomer among the selected top candidates at both PBE0/CRENBL (ECP) level and CCSD(T)/aug-cc-pVDZ (ECP) level of theory (Table S1). The other two isomers are slightly higher (∼0.16 eV) in energy at the CCSD(T)/aug-cc-pVDZ (ECP) level than isomer I while almost degenerate with one another. Despite a systematic shift of around 0.45 eV, isomers I and II can reproduce the X′−A′ and X−A gaps, as well as almost all the main bands. Isomer III can be responsible for the weak features (such as C and D) in the experimental spectrum. Consequently, all three isomers should be present in the cluster beam. Other candidates were easily ruled out because of their relatively high energy at the CCSD(T)/aug-cc-pVDZ (ECP) level of theory or because of notable differences in the theoretical and experimental spectra (Figure S1). Thus, the global minimum of $AuBi_4^-$ probably includes two major isomers, the C_{2v} isomer I and D_{2h} isomer II, along with a minor C_s isomer III. Interestingly, the gold atom of isomer II is coordinated with four Bi atoms, while that of isomers I and III is coordinated with two and one Bi atoms, respectively. Previously reported structures for neutral $AuBi_4$ are completely different from the anions reported here.[32]

$AuBi_5^-$. The 355 nm spectrum of $AuBi_5^-$ (Figure 1d) exhibits three prominent bands (X, A, and B). Two discernible shoulders (X′ and A′) are also observed at around band X. The 266 nm spectrum (Figure 1e) reveals more and congested bands at the higher binding energy side; some are better seen in the 193 nm spectrum (Figure 1f). The weak bands (X′, A′−D′) suggest the existence of a minor isomer.

We examined 10 low-lying structures carefully and found that isomer I was the lowest-energy candidate at all levels of theory (Table S2). Simulated spectra of all the top candidates are presented in Figure S2. On close examination of the theoretical spectra, we observe that the X band and the two overlapping peaks (A and B) along with the peaks at higher binding energy are all well-reproduced by the simulated spectrum of isomer I (Figure 3b). This good agreement between the experiment and the theory is further supported by the 0.096 eV rmsd value of first four peaks (Table S6) and gives credence to the predicted global minimum. Isomer II is about 0.11 eV higher at the CCSD(T) level than isomer I. The theoretical spectrum based on isomer II contains closely spaced features which resemble

DOI: 10.1021/acs.jpcc.8b00166
J. Phys. Chem. C 2018, 122, 6947−6954

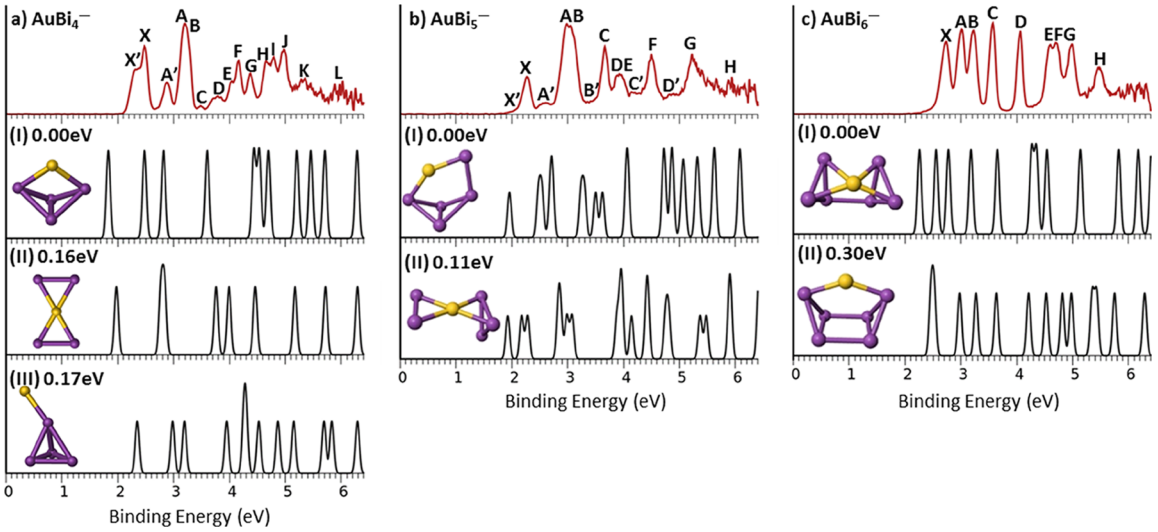

Figure 3. Comparison of the experimental photoelectron spectra (red) of (a) $AuBi_4^-$, (b) $AuBi_5^-$, and (c) $AuBi_6^-$ with simulated spectra (black) of the top candidate isomers (insets display the corresponding isomer structures).

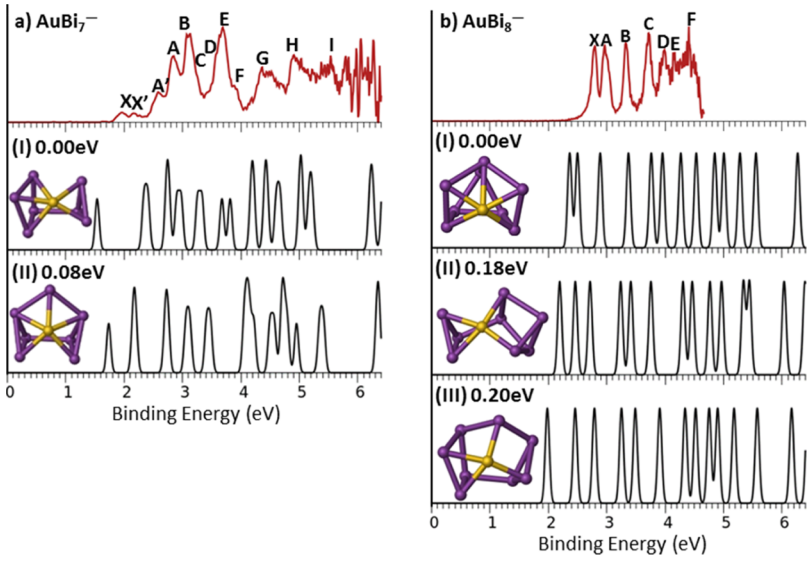

Figure 4. Comparison of the experimental photoelectron spectra (red) of (a) $AuBi_7^-$ and (b) $AuBi_8^-$ with simulated spectra (black) of top candidate isomers (insets display the corresponding isomer structures).

the minor features labeled X′, A′,... of the experimental spectrum. Both isomers I and II are low-symmetry (C_s) structures, which are related to the isomers of $AuBi_4^-$ with one added Bi atom.

$AuBi_6^-$. The 355 nm spectrum of $AuBi_6^-$ (Figure 1g) shows three well-resolved and sharp bands (X, A, and B). Two more sharp bands are observed in the 266 nm spectrum (Figure 1h). The 193 nm spectrum of $AuBi_6^-$ (Figure 1i) reveals four more bands (E−H). Overall, the spectra of $AuBi_6^-$ are well-resolved without minor features observed in other spectra, suggesting that there is only one major isomer present in the cluster beam of $AuBi_6^-$.

We examined a total of 13 low-lying structures and isomers I and II emerged as the top two candidates (Figure 3c). These are the lowest-energy isomers at both the M06/aug-cc-pVTZ (ECP) and PBE0/CRENBL (ECP) levels (Table S3). Other isomers were easily ruled out because of their high relative energies. The theoretical spectra of all the low-lying isomers are presented in Figure S3. The difference in relative energy among the top two isomers is less than 0.09 eV at the PBE0/CRENBL (ECP) level, but at the CCSD(T)/aug-cc-pVDZ (ECP) level isomer I is the lowest in energy and isomer II is 0.30 eV higher. Furthermore, on comparing the theoretical spectra with the experimental spectra, isomer II can be readily ruled out. The simulated spectral pattern of the "bow-tie-like" isomer I is almost in perfect agreement with that of the experiment (rmsd = 0.048 eV, Table S6), providing considerable confidence that the C_s isomer I is the plausible global minimum for $AuBi_6^-$.

$AuBi_7^-$. The 355 nm spectrum of $AuBi_7^-$ (Figure 2a) is quite complicated with both weak (X′ and A′) and intense (X, A−C) bands. The 266 nm spectrum (Figure 2b) exhibits two intense bands (E and G), as well as two shoulders (D and F) on band E. The 193 nm spectrum (Figure 2c) displays two more broad bands (H and I), beyond which the signal/noise ratio became quite poor. As will be shown below, there are at least two isomers contributing to the experimental spectra.

We selected a total of 12 low-lying isomers, many of which are very close in energies, even at the CCSD(T)/aug-cc-pVDZ

DOI: 10.1021/acs.jpcc.8b00166
J. Phys. Chem. C 2018, 122, 6947−6954

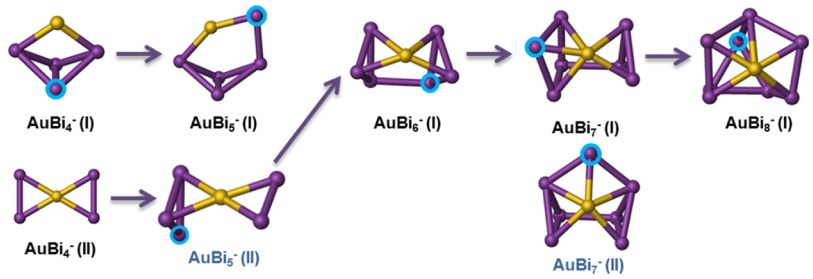

Figure 5. Identified global minimum structures of $AuBi_4^-$ to $AuBi_8^-$ and their structure evolution (black labels: major isomers and blue labels: minor isomers). The gold atom is represented in yellow color, and blue circles represent the additional atom that builds upon the previous cluster.

(ECP) level of theory (Table S4). At the PBE0/CRENBL (ECP) level, the top 10 candidates are within ~0.2 eV of the lowest-energy isomer I. In such cases, a precise spectral match becomes the most important criterion to identify the possible global minimum structure. Upon careful examination of the theoretical spectra (Figure S4), we believe that isomers I and II are the two most promising candidates (Figure 4a). Isomer I is the lowest-energy candidate at all levels of theory, and the spectral features of isomer I agree reasonably well with the major experimental features. Also, the calculated rmsd of first four peaks is only 0.085 eV (Table S6). Isomer II is almost degenerate with isomer I at the CCSD(T) level and seems to produce features labeled X′ and A′. Hence, isomer II is assigned as the minor isomer in the cluster beam. Although both isomers I (C_1) and II (C_s) are low-symmetry structures, they can be viewed as adding one additional Bi atom to the "bow-tie-like" isomer motif of $AuBi_6^-$.

$AuBi_8^-$. The 355 nm spectrum of $AuBi_8^-$ (Figure 2d) displays two intense and closely spaced bands (X and A). Followed by a small energy gap after band A, a weak band B is cut off at the threshold. The 266 nm spectrum of $AuBi_8^-$ (Figure 2e) reveals a well-resolved band B and four more intense bands (C−F). Because of the technical difficulty, we could not acquire 193 nm PES spectra, but we think that the 355 and 266 nm data contained sufficient features to compare with the theory. The well-resolved spectra for $AuBi_8^-$ suggest that the cluster beam most likely contained a single major isomer.

Figure 4b presents the theoretical photoelectron spectra of the top three isomers out of the eight selected candidates (Figure S5). Isomer I is the lowest-energy candidate at both the M06/aug-cc-pVTZ (ECP) and PBE0/CRENBL (ECP) levels of theory (Table S5). At the CCSD(T)/aug-cc-pVDZ (ECP) level, isomer I also exhibits the lowest energy, followed by isomer II. The theoretical spectrum of isomer I reproduces the major features of the experimental spectrum with well-matched relative spacing between the peaks, and rmsd is only 0.054 eV (Table S6). The simulated spectra of the slightly higher energy isomer II are not in good agreement with the experimental spectra. We conclude that isomer I with C_s symmetry is likely the global minimum for $AuBi_8^-$, which can be viewed as adding an additional Bi dimer to the "bow-tie-like" isomer of $AuBi_6^-$.

STRUCTURAL EVOLUTION

The assigned global minima of the $AuBi_n^-$ (n = 4−8) clusters are all low-symmetry structures, as shown in Figure 5. The crystallized Bi_4^{2-} anion is known to be square-planar,[66] and we can view $AuBi_4^-$ as an oxidized species of Bi_4^{2-}. Although one of the $AuBi_4^-$ isomers (II) is a planar structure consisting of two congruent triangles connected by a central gold atom, both the gas-phase isomers I and II are clearly transformed structures and not related to Bi_4^{2-}. The probable evolution of isomers I and II from $AuBi_4^-$ to $AuBi_8^-$ is depicted by arrows in Figure 5. The structures of the larger clusters are more compact as the Au atom becomes more coordinated from $AuBi_6^-$ to $AuBi_8^-$. In fact, in $AuBi_7^-$ and $AuBi_8^-$, the gold atom is coordinated by five bismuth atoms. In Figure 5, we also depict the probable growth of the larger clusters, where the atom circled in blue represents the additional atom that seems to build upon the previous cluster.

It should also be pointed out that in the case of the $AuBi_7^-$ cluster, the two low-lying isomers competing for the global minimum are very close in energy. They are nearly degenerate even at the CCSD(T)/aug-cc-pVDZ (ECP) level of theory, differing in energy only by 0.076 eV, indicating a rather flat potential energy surface. This may be a manifestation of dynamic structural fluxionality, which has been a subject of interest in cluster science. To compare the relative stability of the two isomers of $AuBi_7^-$, we performed BOMD simulations at two different temperatures, 300 and 260 K.

In Figure 6, we present the change in dihedral angle made by atoms (labeled 1−4) during a 5 ps simulation. Isomer I of $AuBi_7^-$ is fairly stable at both temperatures, and its structure remains intact during the simulation (see Movie S1 in the Supporting Information). On the other hand, isomer II is relatively unstable and undergoes structural transformations to isomers that appear like isomers III and IV (Table S4) at both

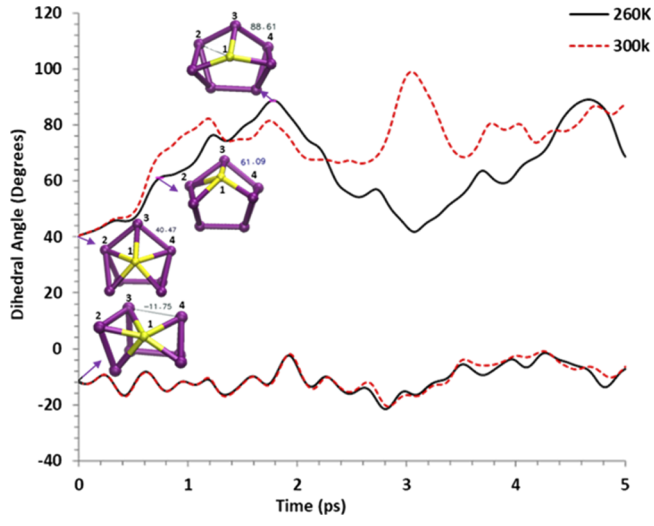

Figure 6. Change in the dihedral angle of atoms (labeled 1−4) in $AuBi_7^-$. Isomer II (top curves) and isomer I (bottom curves) at temperatures 260 and 300 K.

DOI: 10.1021/acs.jpcc.8b00166
J. Phys. Chem. C 2018, 122, 6947−6954

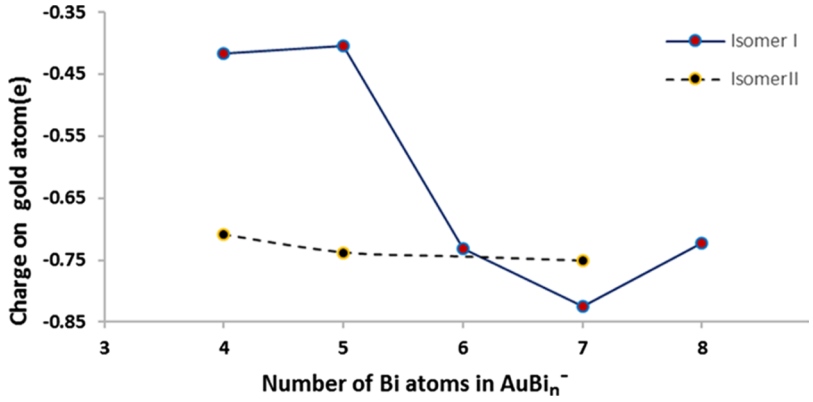

Figure 7. Plot of negative charge on gold with the change in size of the $AuBi_n^-$ clusters.

temperatures, after ~1−2 ps in the simulation (see Movie S2 in the Supporting Information). The snapshots where these isomers appear first in the simulation are presented in Figure 6.

CHARGE DISTRIBUTION AND CHEMICAL BONDING ANALYSES

As gold is more electronegative than bismuth, we expected that there should be charge transfer from Bi to Au in the bimetallic clusters. Indeed, natural population analyses[67] confirmed that more negative charge is localized on the gold atom, but the magnitude of the charge varies with size (Figure 7). The degree of charge transfer depends on the position of the Au atom in the structure, that is, higher coordination results in a higher charge on gold. Specifically, isomer I of both $AuBi_4^-$ and $AuBi_5^-$, which features a two-coordinated gold atom, exhibits a smaller negative charge compared to all other isomers and clusters which contain highly coordinated gold atoms.

We also performed the chemical bonding analyses to better understand the structures and stability of the $AuBi_n^-$ (n = 4−8) clusters. Because of relativistic effects, the 6s orbital of the Bi atom is stabilized and tends not to bond with Au[31,68] Each bismuth atom only employs its 6p electrons to form localized σ or π bonds with neighboring atoms. While the gold atom can occupy both low-coordination and high-coordination sites, it interacts with neighboring bismuth atoms through both localized two-center two-electron (2c-2e) σ bonds and delocalized multicenter two-electron (nc-2e) σ bonds. The bonding analyses are shown in Figure S6 in the Supporting Information. The bonding analyses of $AuBi_4^-$ and $AuBi_5^-$ clearly present a correlation between high coordination of gold atom and delocalization of valence electrons. The low-coordinated $AuBi_4^-$ isomer I consists of seven localized 2c-2e σ bonds with occupation number (ON) of 1.96−1.99 |e|, whereas the high-coordinated isomer II has a delocalized 5c-2e bond with ON = 2 |e| and six 2c-2e σ bonds with ON = 1.76−2.00 |e|. Similarly, isomer I of $AuBi_5^-$ has a low-coordinated gold and consists of eight localized 2c-2e σ bonds with ON = 1.76−1.98 |e|. On the other hand, isomer II has a high-coordinated gold atom and consists of one delocalized 5c-2e σ bond with ON = 1.98 |e| and seven localized 2c-2e σ bonds with ON = 1.72−1.99 |e|. Delocalized bonding is also revealed in $AuBi_n^-$ (n = 6−8) because of the high-coordinated Au. Specifically, the two isomers of $AuBi_7^-$ present considerable differences in their σ bonding framework. Isomer I has three 3c-2e σ bonds with ON = 1.78−1.94 |e|, whereas isomer II exhibits delocalization consisting of one 3c-1e ON = 1.00 |e|, one 3c-2e ON = 1.97 |e|, and 4c-2e ON = 1.89 |e| σ bonds.

CONCLUSIONS

We have performed a combined PES and DFT study on a series of Au-doped bismuth clusters $AuBi_n^-$ (n = 4−8). Low-symmetry three-dimensional (3D) structures are prevalent in this size range, although a planar isomer coexists with the 3D global minimum for $AuBi_4^-$. The gold atom prefers low-coordination sites in 3D structures for n = 4 and 5, but increasingly high-coordination sites prevail from n = 6−8. $AuBi_6^-$ has a stable global minimum with a "bow-tie-like" structure, and the major isomers of other clusters also possess this motif. Chemical bonding analyses reveal that the gold atom interacts with neighboring bismuth atoms through localized σ bonds at low-coordination sites but through delocalized σ bonds at high-coordination sites. This trend of local coordination in turn is directly correlated to the atomic charge localization on the gold atom, that is, the higher the coordination number of gold, the greater is the localized negative charge on gold. BOMD simulations suggest that the major isomer of $AuBi_7^-$ is stable at 260 and 300 K, whereas the minor isomer shows a fluxional behavior and structural transformation at these temperatures.

ASSOCIATED CONTENT

Supporting Information

The Supporting Information is available free of charge on the ACS Publications website at DOI: 10.1021/acs.jpcc.8b00166.

Energy tables, simulated and experimental photoelectron spectra for all the top candidate isomers of $AuBi_n^-$ (n = 4−8), and rmsd of simulated spectra of the major isomers (PDF)

Fairly stable isomer I of $AuBi_7^-$ with its intact structure during the simulation (MPG)

Relatively unstable isomer II of $AuBi_7^-$ undergoing structural transformations to isomers that appear like isomers III and IV (MPG)

AUTHOR INFORMATION

Corresponding Authors

*E-mail: Lai-Sheng_Wang@brown.edu (L.-S.W.).
*E-mail: xzeng1@unl.edu (X.C.Z.).

ORCID

Lai-Sheng Wang: 0000-0003-1816-5738

DOI: 10.1021/acs.jpcc.8b00166
J. Phys. Chem. C 2018, 122, 6947−6954

Xiao Cheng Zeng: 0000-0003-4672-8585

Author Contributions

‖These authors contributed equally to this work.

Notes

The authors declare no competing financial interest.

■ ACKNOWLEDGMENTS

The experiment done at Brown University was supported by the National Science Foundation (CHE-1632813 to L.-S.W.). X.C.Z. was supported by a grant from Nebraska Center for Energy Sciences Research. The calculations were performed at the Holland Computing Center, University of Nebraska-Lincoln. T.J. would like to thank Dr. Wei-Li Li and Dr. Gary V. Lopez for earlier experimental assistance.

■ REFERENCES

(1) Ferrando, R.; Jellinek, J.; Johnston, R. L. Nanoalloys: From Theory to Applications of Alloy Clusters and Nanoparticles. *Chem. Rev.* **2008**, *108*, 845−910.
(2) Andrews, M. P.; O'brien, S. C. Gas-Phase " Molecular Alloys" of Bulk Immlscible Elements: Fe_xAg_y. *J. Phys. Chem.* **1992**, *96*, 8233−8241.
(3) Wang, D.; Villa, A.; Porta, F.; Prati, L.; Su, D. Bimetallic Gold/Palladium Catalysts: Correlation between Nanostructure and Synergistic Effects. *J. Phys. Chem. C* **2008**, *112*, 8617−8622.
(4) Liu, J.-H.; Wang, A.-Q.; Chi, Y.-S.; Lin, H.-P.; Mou, C.-Y. Synergistic Effect in an Au−Ag Alloy Nanocatalyst: CO Oxidation. *J. Phys. Chem. B* **2005**, *109*, 40−43.
(5) Gupta, U.; Reber, A. C.; Clayborne, P. A.; Melko, J. J.; Khanna, S. N.; Castleman, A. W. Effect of Charge and Composition on the Structural Fluxionality and Stability of Nine Atom Tin−Bismuth Zintl Analogues. *Inorg. Chem.* **2008**, *47*, 10953−10958.
(6) Vossloh, C.; Holdenried, M.; Micklitz, H. Influence of Cluster Size on the Normal- and Superconducting-State Properties of Granular Bi Films. *Phys. Rev. B: Condens. Matter Mater. Phys.* **1998**, *58*, 12422−12426.
(7) Süzer, S.; Lee, S.-T.; Shirley, D. A. PES of Atomic and Molecular Bismuth. *J. Chem. Phys.* **1976**, *65*, 412−417.
(8) Kajita, A.; Saito, Y.; Yasue, T.; Hayashi, M.; Ichimiya, A.; Gotoh, T.; Kawaguchi, Y.; Kotani, M.; Shigeta, Y.; Takagi, S.; et al. Threshold Behavior of Synchrotron Radiation Photoionization for Bi_n($n \leq 4$). *J. Phys. Soc. Jpn.* **1989**, *58*, 2320−2324.
(9) Saito, Y.; Kajita, A.; Yasue, T.; Hayashi, M.; Ichimiya, A.; Gotoh, T.; Kawaguchi, Y.; Kotani, M.; Shigeta, Y.; Takagi, S.; et al. Photoionization Efficiency Curves in the Threshold Region for Bi_n($n \leq 4$)molecules. *Phys. Scr.* **1990**, *41*, 51−54.
(10) Wang, L.-S.; Lee, Y. T.; Shirley, D. A.; Balasubramanian, K.; Feng, P. Photoelectron Spectroscopy and Electronic Structure of Clusters of the Group V Elements. I. Dimers. *J. Chem. Phys.* **1990**, *93*, 6310−6317.
(11) Polak, M. L.; Ho, J.; Gerber, G.; Lineberger, W. C. Photoelectron Spectroscopy of Negatively Charged Bismuth Clusters: Bi_2^-, Bi_3^-, and B_4^-. *J. Chem. Phys.* **1991**, *95*, 3053−3063.
(12) Böwering, N.; Martins, M.; Snell, G.; Kuntze, R.; Heinzmann, U. Spin-Resolved Photoelectron Spectroscopy in the Autoionization Region of Atomic Bismuth. *J. Phys. B: At., Mol. Opt. Phys.* **1998**, *31*, 5221−5232.
(13) Zhai, H.-J.; Wang, L.-S.; Kuznetsov, A. E.; Boldyrev, A. I. Probing the Electronic Structure and Aromaticity of Pentapnictogen Cluster Anions Pn_5^- (Pn = P, As, Sb, and Bi) Using Photoelectron Spectroscopy and Ab Initio Calculations. *J. Phys. Chem. A* **2002**, *106*, 5600−5606.
(14) Mikkelä, M.-H.; Tchaplyguine, M.; Urpelainen, S.; Jänkälä, K.; Björneholm, O.; Huttula, M. Photoelectron Spectroscopy of Unsupported Bismuth Clusters: Size Related Effects of Metallic Properties. *J. Appl. Phys.* **2012**, *112*, 084326.
(15) Balasubramanian, K.; Liao, D.-W. Spectroscopic Constants and Potential Energy Curves of Bi_2 and Bi^-_2. *J. Chem. Phys.* **1991**, *95*, 3064−3073.
(16) Balasubramanian, K.; Sumathi, K.; Dai, D. Group V Trimers and Their Positive Ions: The Electronic Structure and Potential Energy Surfaces. *J. Chem. Phys.* **1991**, *95*, 3494−3505.
(17) Choi, H.; Park, C.; Baeck, K. K. Ab Initio Study of the Geometries and Vibrational Properties of the Low-Lying Electronic States of Neutral and Anionic M_3 (M = P, As, Sb, and Bi): The Photoelectron Spectroscopy of the Anions. *J. Phys. Chem. A* **2002**, *106*, 5177−5187.
(18) Gao, L.; Li, P.; Lu, H.; Li, S. F.; Guo, Z. X. Size- and Charge-Dependent Geometric and Electronic Structures of B_{in} (B_{in}^-) Clusters (n=2-13) by First-Principles Simulations. *J. Chem. Phys.* **2008**, *128*, 194304.
(19) Yuan, H. K.; Chen, H.; Kuang, A. L.; Miao, Y.; Xiong, Z. H. Density-Functional Study of Small Neutral and Cationic Bismuth Clusters Bi_n and Bi_n^+(n=2−24). *J. Chem. Phys.* **2008**, *128*, 094305.
(20) Jia, J. M.; Chen, G. B.; Shi, D. N.; Wang, B. L. Structural and Electronic Properties of Bi_n (n = 2-14) Clusters from Density-Functional Calculations. *Eur. Phys. J. D* **2008**, *47*, 359−365.
(21) Gausa, M.; Kaschner, R.; Seifert, G.; Faehrmann, J. H.; Lutz, H. O.; Meiwes-Broer, K.-H. Photoelectron Investigations and Density Functional Calculations of Anionic Sb_n^- and Bi_n^- Clusters. *J. Chem. Phys.* **1996**, *104*, 9719−9728.
(22) Kelting, R.; Baldes, A.; Schwarz, U.; Rapps, T.; Schooss, D.; Weis, P.; Neiss, C.; Weigend, F.; Kappes, M. M. Structures of Small Bismuth Cluster Cations. *J. Chem. Phys.* **2012**, *136*, 154309.
(23) Sun, S.; Liu, H.; Tang, Z. Experimental and Theoretical Investigation on Binary Semiconductor Clusters of Bi/Si, Bi/Ge, and Bi/Sn. *J. Phys. Chem. A* **2006**, *110*, 5004−5009.
(24) Clayborne, P. A.; Gupta, U.; Reber, A. C.; Melko, J. J.; Khanna, S. N.; Castleman, A. W. The Applicability of Three-Dimensional Aromaticity in $BiSn_n^-$ Zintl Analogues. *J. Chem. Phys.* **2010**, *133*, 134302.
(25) Melko, J. J.; Werner, U.; Mitrić, R.; Bonačic-Koutecky, V.; Castleman, A. W. Electronic Structure Similarities in $Pb_xSb_y^-$ and $Sn_xBi_y^-$ Clusters. *J. Phys. Chem. A* **2011**, *115*, 10276−10280.
(26) Sun, Z.; Xu, H.-G.; Feng, G.; Xu, X.-L.; Zheng, W.-J. Photoelectron Spectroscopy and Density Functional Theory Study of $Bi_2Al_n^-$ (n=1−4) Clusters. *Chem. Phys. Lett.* **2014**, *615*, 56−61.
(27) Gupta, U.; Reveles, J. U.; Melko, J. J.; Khanna, S. N.; Castleman, A. W. Origins of Stability in Mixed Bismuth-Indium Clusters. *J. Phys. Chem. C* **2010**, *114*, 15963−15972.
(28) Sobhy, M. A.; Reveles, J. U.; Gupta, U.; Khanna, S. N.; Castleman, A. W. Photoelectron Imaging and Theoretical Investigation of Bimetallic Bi_{1-2} Ga_{0-2}^- and Pb_{1-4}^- Cluster Anions. *J. Chem. Phys.* **2009**, *130*, 054304.
(29) Sun, Z.; Zhu, Q.; Gao, Z.; Tang, Z. Experimental and Theoretical Investigation on Binary Anionic Clusters of $Al_mBi_n^-$. *Rapid Commun. Mass Spectrom.* **2009**, *23*, 2663−2668.
(30) Jian, T.; Cheung, L. F.; Chen, T.-T.; Wang, L.-S. Bismuth-Boron Multiple Bonding in BiB_2O^- and Bi_2B^-. *Angew. Chem., Int. Ed.* **2017**, *56*, 9551−9555.
(31) Jian, T.; Lopez, G. V.; Wang, L.-S. Photoelectron Spectroscopy of $BiAu^-$ and $BiBO^-$: Further Evidence of the Analogy between Au and Boronyl. *J. Phys. Chem. B* **2016**, *120*, 1635−1640.
(32) Seifried, C.; Longo, L.; Pollak, P.; Weigend, F. The Chemical Space of Pb_{N-n} Bi_n and $(Pb_{N-n}$ $Bi_n)^+$: A Systematic Study for N = 3−13. *J. Chem. Phys.* **2017**, *146*, 034304.
(33) Chen, H.; Yuan, H. K.; Kuang, A. L.; Miao, Y.; Chen, P.; Xiong, Z. H. Geometrical Evolution, Electronic Structures, and Magnetic Properties of Bi-Mn Binary Clusters. *Phys. Rev. B: Condens. Matter Mater. Phys.* **2008**, *77*, 184429.
(34) Huang, S.-Y.; Xie, Z.; Ma, Q.-M.; Liu, Y.; Li, Y.-C. Geometries, Electronic Structures, and Magnetism of Small Bi_mCo_n Clusters. *J. Mol. Struct.: THEOCHEM* **2010**, *953*, 103−113.

DOI: 10.1021/acs.jpcc.8b00166
J. Phys. Chem. C 2018, 122, 6947−6954

(35) Rangel, E.; Sansores, L. E. Theoretical Study of Neutral Bismuth-Copper, Bismuth-Silver and Bismuth-Gold Clusters. *Eur. Phys. J. D* **2013**, *67*, 239.
(36) Martínez, A. Gold−Bismuth Clusters. *J. Phys. Chem. A* **2014**, *118*, 5894−5902.
(37) Clarke, S. M.; Amsler, M.; Walsh, J. P. S.; Yu, T.; Wang, Y.; Meng, Y.; Jacobsen, S. D.; Wolverton, C.; Freedman, D. E. Creating Binary Cu−Bi Compounds via High-Pressure Synthesis: A Combined Experimental and Theoretical Study. *Chem. Mater.* **2017**, *29*, 5276−5285.
(38) Miralrio, A.; Hernández-Hernández, A.; Pescador-Rojas, J. A.; Sansores, E.; López-Pérez, P. A.; Martínez-Farías, F. Rangel Cortes, E. Theoretical Study of the Stability and Properties of Magic Numbers (m = 5, n = 2) and (m = 6, n = 3) of Bimetallic Bismuth-Copper Nanoclusters; Bi_m Cu_n. *Int. J. Quantum Chem.* **2017**, *117*, No. e25449.
(39) Heiles, S.; Hofmann, K.; Johnston, R. L.; Schäfer, R. Nine-Atom Tin-Bismuth Clusters: Mimicking Excess Electrons by Element Substitution. *ChemPlusChem* **2012**, *77*, 532−535.
(40) Heiles, S.; Johnston, R. L.; Schäfer, R. Bismuth-Doped Tin Clusters: Experimental and Theoretical Studies of Neutral Zintl Analogues. *J. Phys. Chem. A* **2012**, *116*, 7756−7764.
(41) Wang, L.-M.; Bai, J.; Lechtken, A.; Huang, W.; Schooss, D.; Kappes, M. M.; Zeng, X. C.; Wang, L.-S. Magnetic Doping of the Golden Cage Cluster M@Au16− (M=Fe,Co,Ni). *Phys. Rev. B: Condens. Matter Mater. Phys.* **2009**, *79*, 33413.
(42) Pal, R.; Wang, L.-M.; Huang, W.; Wang, L.-S.; Zeng, X. C. Structural Evolution of Doped Gold Clusters: MAu_x^- (M = Si, Ge, Sn; X = 5−8). *J. Am. Chem. Soc.* **2009**, *131*, 3396−3404.
(43) Wang, L.-M.; Bulusu, S.; Huang, W.; Pal, R.; Wang, L.-S.; Zeng, X. C. Doping the Golden Cage Au_{16}^- with Si, Ge, and Sn. *J. Am. Chem. Soc.* **2007**, *129*, 15136−15137.
(44) Wang, L.-M.; Bulusu, S.; Zhai, H.-J.; Zeng, X.-C.; Wang, L.-S. Doping Golden Buckyballs: $Cu@Au_{16}^-$ and $Cu@Au_{17}^-$ Cluster Anions. *Angew. Chem., Int. Ed.* **2007**, *46*, 2915−2918.
(45) Wang, L.-M.; Pal, R.; Huang, W.; Zeng, X. C.; Wang, L.-S. Tuning the Electronic Properties of the Golden Buckyball by Endohedral Doping. *J. Chem. Phys.* **2009**, *130*, 051101.
(46) Haruta, M.; Kobayashi, T.; Sano, H.; Yamada, N. Novel Gold Catalysts for the Oxidation of Carbon Monoxide at a Temperature Far below 0°C. *Chem. Lett.* **1987**, *16*, 405−408.
(47) Wang, L.-S.; Cheng, H.-S.; Fan, J. Photoelectron Spectroscopy of Size-selected Transition Metal Clusters: Fe_n^-, n = 3−24. *J. Chem. Phys.* **1995**, *102*, 9480−9493.
(48) Wang, L.-S. Photoelectron Spectroscopy of Size-Selected Boron Clusters: From Planar Structures to Borophenes and Borospherenes. *Int. Rev. Phys. Chem.* **2016**, *35*, 69−142.
(49) Wales, D. J.; Doye, J. P. K. Global Optimization by Basin-Hopping and the Lowest Energy Structures of Lennard-Jones Clusters Containing up to 110 Atoms. *J. Phys. Chem. A* **1997**, *101*, 5111−5116.
(50) Heiles, S.; Johnston, R. L. Global Optimization of Clusters Using Electronic Structure Methods. *Int. J. Quantum Chem.* **2013**, *113*, 2091−2109.
(51) Perdew, J. P.; Burke, K.; Ernzerhof, M. Generalized Gradient Approximation Made Simple. *Phys. Rev. Lett.* **1996**, *77*, 3865−3868.
(52) Delley, B. From Molecules to Solids with the DMol3 Approach. *J. Chem. Phys.* **2000**, *113*, 7756−7764.
(53) Zhao, Y.; Truhlar, D. G. The M06 Suite of Density Functionals for Main Group Thermochemistry, Thermochemical Kinetics, Noncovalent Interactions, Excited States, and Transition Elements: Two New Functionals and Systematic Testing of Four M06-Class Functionals and 12 Other Function. *Theor. Chem. Acc.* **2008**, *120*, 215−241.
(54) Kendall, R. A.; Dunning, T. H., Jr.; Harrison, R. J. Electron Affinities of the First-Row Atoms Revisited. Systematic Basis Sets and Wave Functions. *J. Chem. Phys.* **1992**, *96*, 6796−6806.
(55) Peterson, K. A.; Puzzarini, C. Systematically Convergent Basis Sets for Transition Metals. II. Pseudopotential-Based Correlation Consistent Basis Sets for the Group 11 (Cu, Ag, Au) and 12 (Zn, Cd, Hg) Elements. *Theor. Chem. Acc.* **2005**, *114*, 283−296.
(56) Metz, B.; Stoll, H.; Dolg, M. Small-Core Multiconfiguration-Dirac−Hartree−Fock-Adjusted Pseudopotentials for Post- D Main Group Elements: Application to PbH and PbO. *J. Chem. Phys.* **2000**, *113*, 2563−2569.
(57) Frisch, M. J.; Trucks, G. W.; Schlegel, H. B.; Scuseria, G. E.; Robb, M. A.; Cheeseman, J. R.; Scalmani, G.; Barone, V.; Mennucci, B.; Petersson, G. A.; et al. *Gaussian 09*, Revision E.01; Gaussian, Inc.: Wallingford CT, 2009.
(58) Johansson, M. P.; Lechtken, A.; Schooss, D.; Kappes, M. M.; Furche, F. 2D-3D Transition of Gold Cluster Anions Resolved. *Phys. Rev. A: At., Mol., Opt. Phys.* **2008**, *77*, 53202.
(59) Pande, S.; Huang, W.; Shao, N.; Wang, L.-M.; Khetrapal, N.; Mei, W.-N.; Jian, T.; Wang, L.-S.; Zeng, X. C. Structural Evolution of Core-Shell Gold Nanoclusters: Au_n^-(n = 42-50). *ACS Nano* **2016**, *10*, 10013−10022.
(60) Khetrapal, N. S.; Jian, T.; Pal, R.; Lopez, G. V.; Pande, S.; Wang, L.-S.; Zeng, X. C. Probing the Structures of Gold−aluminum Alloy Clusters $Au_xAl_y^-$: A Joint Experimental and Theoretical Study. *Nanoscale* **2016**, *8*, 9805−9814.
(61) Khetrapal, N. S.; Jian, T.; Lopez, G. V.; Pande, S.; Wang, L.-S.; Zeng, X. C. Probing the Structural Evolution of Gold−Aluminum Bimetallic Clusters ($Au_2Al_n^-$, n = 3−11) Using Photoelectron Spectroscopy and Theoretical Calculations. *J. Phys. Chem. C* **2017**, *121*, 18234−18243.
(62) Adamo, C.; Barone, V. Toward Reliable Density Functional Methods without Adjustable Parameters: The PBE0 Model. *J. Chem. Phys.* **1999**, *110*, 6158−6170.
(63) Ross, R. B.; Powers, J. M.; Atashroo, T.; Ermler, W. C.; LaJohn, L. A.; Christiansen, P. A. Ab Initio Relativistic Effective Potentials with Spin−orbit Operators. IV. Cs through Rn. *J. Chem. Phys.* **1990**, *93*, 6654.
(64) Valiev, M.; Bylaska, E. J.; Govind, N.; Kowalski, K.; Straatsma, T. P.; Van Dam, H. J. J.; Wang, D.; Nieplocha, J.; Apra, E.; Windus, T. L.; et al. NWChem: A Comprehensive and Scalable Open-Source Solution for Large Scale Molecular Simulations. *Comput. Phys. Commun.* **2010**, *181*, 1477−1489.
(65) The CP2K Developers Group, 2004.
(66) Kuznetsov, A. N.; Fässler, T. F. Bismuth Polyanions in Solution: Synthesis and Structural Characterization of $(2, 2, 2\text{-Crypt-A})_2Bi_4$ (A = K, Rb) and the Formation of the Laves Phases ABi_2 (A = K, Rb, Cs) from Solution. *Z. Anorg. Allg. Chem.* **2002**, *628*, 2537−2541.
(67) Reed, A. E.; Weinstock, R. B.; Weinhold, F. Natural Population Analysis. *J. Chem. Phys.* **1985**, *83*, 735−746.
(68) Pyykko, P. Relativistic Effects in Structural Chemistry. *Chem. Rev.* **1988**, *88*, 563−594.
(69) Zubarev, D. Y.; Boldyrev, A. I. Developing paradigms of chemical bonding: adaptive natural density partitioning. *Phys. Chem. Chem. Phys.* **2008**, *10*, 5207−5217.

DOI: 10.1021/acs.jpcc.8b00166
J. Phys. Chem. C 2018, 122, 6947−6954